Cluster, backbone, and elastic backbone structures of the multiple invasion percolation

Roberto N. Onody and Reginaldo A. Zara
Departamento de Física e Informática, Instituto de Física de São Carlos, Universidade de São Paulo, Caixa Postal 369, 13560-970 São Carlos, São Paulo, Brazil

(Received 19 February 1997; revised manuscript received 13 May 1997)

We study the cluster, the backbone, and the elastic backbone structures of the multiple invasion percolation for both the perimeter and the optimized versions. We investigate the behavior of the mass, the number of red sites (i.e., sites through which all the current passes), and loops of those structures. Their corresponding scaling exponents are also estimated. By construction, the mass of the optimized model scales exactly with the gyration radius of the cluster—we verify that this also happens to the backbone. Our simulation shows that the red sites almost disappear, indicating that the cluster has achieved a high degree of connectivity. [S1063-651X(97)14908-X]

PACS number(s): 64.60.Ak, 64.60.Cn, 05.50.+q

I. INTRODUCTION

When a nonviscous liquid is injected into a porous medium already filled with a viscous fluid two distinct regimes appear: one where the dominant forces are of *capillary* nature and another where the *viscous* forces are predominant. Depending on the injection rate the system can be found in one of these regimes. The theoretical description of such a system is based on two models: invasion percolation [1] and diffusion-limited aggregation (DLA) [2]. The invasion percolation model is indicated when the fluid flow is slow, that is, when the capillary number is small. The displacement process of the fluid follows minimum resistance paths: the smaller pores are filled or invaded first.

Grassberger and Manna [3] pointed out that the invasion percolation is a kind of self-organizing criticality [4] exhibiting scale invariant behavior in time and space and evolving into a natural critical state. Indeed, there are two kinds of invasion percolation models: *with* and *without* trapping [1]. The trapping occurs when the displaced fluid is an uncompressible fluid and it is completely surrounded by the other. These models belong to different universality class. The version with trapping has a fractal dimension $D_F \sim 1.82$ and the case without trapping corresponds to the *critical ordinary percolation* [1] ($D_F = \frac{91}{48}$). Important applications of the invasion percolation model were found, extending from the terciary recovery of petroleum to the fingering phenomena in soils [5].

Many modifications of the original invasion percolation model have been proposed. They take into account the action of an external gravitational field [6–8] or the flux with a privileged direction [9]. In the pioneer formulation of the invasion percolation model [1], at each growth step only *one* lattice site was allowed to be occupied. Recently [10], a more realistic model was investigated, which permits that a certain number of lattice sites can be invaded at the same time: the *multiple invasion percolation* model. There are two kinds of multiple invasion percolation: the perimeter model and the optimized model. In the first model the cluster growth is controlled by the flux through the perimeter. The optimized model is governed by a scaling relation between the mass and the gyration radius of the cluster. Reference [10] studied the multiple invasion percolation (in its *site* version, as in this paper) determining the abundance of vertice type, the mean coordination number, the acceptance profile, and the fractal dimensions. An interesting *burst* phenomenon was detected and analyzed in the optimized model.

The backbone is the intersection of *all* self-avoiding walks connecting two points P_1 and P_2 of the lattice. This means that if we pass a current between P_1 and P_2 the backbone is the set of points carrying current, and all dangling ends are discarded. The elastic backbone is the union of all the shortest paths between P_1 and P_2. In our case P_1 is the lattice center and P_2 is the point where the cluster finds the frontier for the first time (the growth process stops at this moment). The investigation of the backbone of clusters has been of interest for a long time. Possible applications are the conductivity of random systems [11] and the flow of fluids in porous media [12].

The cluster, the backbone, and the elastic backbone are the important *structures* of the fractal objects. The determination of the properties of such structures can lead to a better understanding of the fractal objects and even to a classification scheme for them. But what are the relevant parameters to be measured in these structures? We can list the following quantities: the mass, the minimum path, the number of red points (i.e., points through which all the current passes), and the number of loops. At criticality, all of them scale as a power law with the lattice size. So they can be characterized by their corresponding scaling exponents.

The minimum path is the shortest distance between two lattice points. The lengths of the minimum path or ''chemical distance'' are usually greater than their Euclidean distance [13]. The red points are the throttle points through which all the current passes—if they are removed the flow stops.

In the present paper we study the cluster, the backbone, and the elastic backbone structures of the multiple invasion percolation for both the perimeter and optimized models. To determine the backbone and the elastic backbone we employed the burning algorithm [14]. Although there are actually more efficient algorithms based on artificial intelligence theory [15] or recursive algorithm [16], we prefer the burning technique because beyond the backbone and elastic back-

bone identification it also permits the determination of the red sites and loops.

The scaling exponents for the mass, the red sites, the minimum path, and the loops are found for many values of the parameters F and D of the perimeter and the optimized models. We did not strive to make these exponents very precise. Indeed we paid more attention to the physical changes occurring with the variation of the parameters, as long as both models were conceived to continuously interpolate from fractal to compact objects. The optimized model reveals two amazing properties: not only the cluster but also the backbone mass scales *exactly* with the gyration radius and the red points practically do not exist anymore. This means that the cluster, generated with the optimized algorithm, has acquired a high degree of connectivity without having to increase its fractal dimension.

II. THE PERIMETER MODEL

We briefly recall the growth mechanism established for the perimeter model. Suppose that at some growth stage t the cluster mass is M_t and the rectangle area inside which the cluster is inscribed is A. The square root of A can be interpreted as a measure of the correlation length [17]. This interpretation comes from the fact that, as in the ordinary invasion percolation, the multiple invasion percolation can also be thought of as a kind of critical percolation model [10]. At time $t+1$, the cluster mass M_{t+1} will be given by

$$M_{t+1}=M_t+\mathrm{Int}(4F\sqrt{A}), \tag{1}$$

where Int means the integer part, and F is an external parameter ($0\leqslant F\leqslant 1$) corresponding to the fraction of the perimeter $4\sqrt{A}$ to be invaded at time $t+1$. We start the growing process at the center of a square lattice.

It was numerically shown in Ref. [10] that for F values greater than 1/2 the cluster is compact and for $0\leqslant F\leqslant 0.5$ it interpolates between the ordinary invasion percolation (with fractal dimension $D_F=\frac{91}{48}$) and the closed-packed limit ($D_F=2$). We found a simple analytic demonstration of this fact. For a lattice size L, a cluster growing *compactly* from its center will touch the boundary at a time $t=L/2$ and it will acquire the form of a square with side $l=L/\sqrt{2}$. The mass is $M_t=L^2/2$. At time $t+1$, *all* available sites will be invaded and the maximum possible mass is $M_{t+1}=(L+2)^2/2$. Using Eq. (1) we have the inequality

$$F\leqslant\frac{1}{2}+\frac{1}{2L}, \tag{2}$$

which for large lattices saturates at $F=\frac{1}{2}$.

In order to obtain the scaling exponents, throughout this section we use lattices of size $L=51$, 101, 201, and 401.

A. The mass

The mass of fractal objects [18] scales with the lattice size L as

$$M\sim L^{D_F}. \tag{3}$$

TABLE I. The scaling exponents of the perimeter model. The order they appear in this table corresponds to the cluster, backbone, and elastic backbone, respectively. Those marked with an asterisk were calculated using the ratio method.

F	D_F	D_r	D_l	$D_{\min}$
	1.88(1)	0.77(2)*	1.98(1)	
0.0	1.64(1)	0.77(2)*	1.72(1)	1.14(4)*
	1.17(4)*	1.08(5)*	1.19(1)	
	1.98(1)	0.38(6)*	1.99(1)	
0.1	1.89(2)	0.38(6)*	1.92(1)	1.05(1)*
	1.05(2)*	1.10(2)*	1.17(1)	
	1.99(1)	0.29(6)*	1.99(1)	
0.2	2.00(2)	0.29(6)*	2.00(2)	1.05(1)*
	1.02(2)*	1.08(2)*	1.11(1)	
	1.98(1)	0.07(4)*	1.95(1)	
0.3	2.00(1)	0.07(4)*	1.94(3)	1.04(1)*
	1.03(3)*	1.03(3)*	1.12(1)	
	1.99(1)	0.05(4)*	1.97(1)	
0.4	2.00(1)	0.05(4)*	1.97(4)	1.02(1)*
	1.01(4)*	1.01(3)*	1.00(3)	

The cluster mass, the fractal dimension, and its dependence on F were already studied [10]. Here we extend the results to the backbone and the elastic backbone. The data for the backbone are of good quality and they were obtained by averaging over 100–2000 realizations. We get, for example, $D_F(F=0)=1.64\pm 0.01$, which is completely compatible with the most extensive simulation performed by Grassberger [16], who got 1.647 ± 0.004. Our results are shown in Table I. With increasing F the backbone fractal dimension goes to 2 in a faster way than those of the cluster itself. From Table I we see that around $F\sim 0.3$ some exponents break their monotonic behavior. At this point the cluster has a circular form and the corresponding gyration radius is maximum [10].

For the elastic backbone we found deviations from the straight line when we plotted $\ln(M)\ln(L)$. This strongly indicates that corrections to scaling are necessary. We adopted the ratio method [13] to correct them. For $F=0$ we got $D_F=1.17\pm 0.04$, which is in fair agreement with the result of Herrmann *et al.* [14]: 1.10 ± 0.05. When F increases, the trend is that the elastic backbone approaches the form of a straight line connecting the lattice center to the point where the cluster hits the frontier. The mass exponent goes to one.

B. The red sites

The number of red sites N_r scales as

$$N_r\sim L^{D_r}. \tag{4}$$

Here again corrections to scaling are necessary. Of course, the exponents D_r for the cluster and the backbone are the same. In the case of the ordinary invasion percolation ($F=0$), D_r is known exactly [19]. Coniglio used the relations between the percolation model, Potts model, and Coulomb gas to get $D_r=\frac{3}{4}$. Our result $D_r(F=0)=0.77\pm 0.02$ is in good agreement. As F goes to 0.5 the exponent D_r approaches zero (see Table I). For the elastic backbone we get

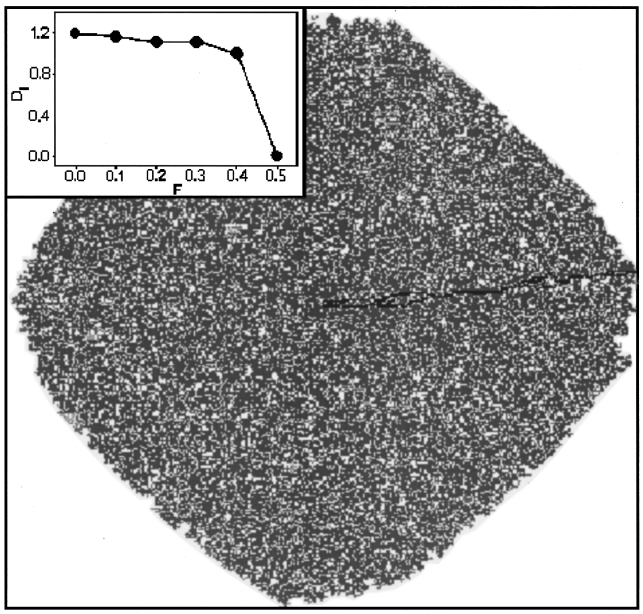

FIG. 1. In gray is a typical cluster of the perimeter model with $F=0.4$ on a lattice of size $L=401$. The elastic backbone is shown in black. The inset gives the dependence of the loop number scaling exponent with F.

$D_r(F=0)=1.08\pm0.05$. As we have already observed, the elastic backbone approaches a straight line with increasing F. This means that almost every site belonging to the elastic backbone is a red site, so $D_r \sim D_F \rightarrow 1$ as F goes to 0.5.

C. The loops

We can put a bond connecting any two nearest-neighbor occupied sites. The result is a connected graph for which the Euler relation holds: $N_l = N_b - M + 1$, where N_l is the number of cycles or loops; N_b is the number of bonds and M is the mass or the number of sites. For the burning algorithm on the square lattice, N_l is calculated by counting the number of times that one tries to burn a site that is already burned in the same time unit.

The number of loops N_l scales with the lattice size L as

$$N_l \sim L^{D_l}. \tag{5}$$

The data are of very good quality and no correction to scaling was necessary. The exponent D_l approaches 2 with increasing F for both the cluster and the backbone. This is a consequence of the Euler relation. As F increases, the clusters become more compact, N_b approaches $2M$, and, for large clusters, $N_l \sim M \sim L^2$. On the other hand, looking at Table I, the exponent seems to approach 1 for the elastic backbone but this not true. In Fig. 1 we show one typical cluster with $F=0.4$ and $L=401$. The elastic backbone starts at the center and follows to the right nearly as a straight line until it finds an obstacle (a site with a large random number associated). Then a kind of jet appears, which increases the number of loops. In the limit $L \rightarrow \infty$ such an effect can only be avoided if $F \geqslant 0.5$. This means that for the elastic backbone D_l goes abruptly to zero near $F \sim 0.5$ as shown in the inset of Fig. 1.

TABLE II. The ratio N_p/N_0 measures how many times the number of experiments in the perimeter model N_p exceeds that of the optimized N_o when we impose they have the same relative standard deviation $\Delta M/M$. The first and the second lines correspond to the cluster and the backbone, respectively. We used $N_o(L=51,101)=100$, $N_o(L=201)=15$.

L	$\Delta M/M$	N_p/N_o
51	0.009	21
	0.013	10
101	0.009	24
	0.013	13
201	0.017	36
	0.022	25

D. The minimum path

The minimum path scales as

$$l_{\min} \sim L^{D_{\min}}. \tag{6}$$

Naturally, the exponent $D_{\min}$ is the same for the cluster, backbone, and elastic backbone. Our estimate $D_{\min}(F=0)=1.14\pm0.04$ is consistent with the most precise value $D_{\min}=1.1307\pm0.0004$ [16]. We see from Table I that $D_{\min}$ approaches 1 with increasing F.

III. THE OPTIMIZED MODEL

The optimized model [10] was devised in order to have a growth mechanism obeying *exactly* the scaling

$$M \sim (R_g)^D \tag{7}$$

or as near to it as possible (R_g is the gyration radius and D is a real positive external parameter that can be tuned).

Basically we use the following strategy: at *each* growing step we have a list containing *all* the cluster perimeter sites that can be invaded and we seek the number of sites that should be invaded in order that Eq. (7) is verified as closely as possible. This proceeding builds a fractal object that is extremely stabilized in the sense that in *any* stage or size the scaling is perfectly obeyed not only in the asymptotic limit (as usual). Another important advantage is that the necessity of mass averages on the cluster ensemble diminishes. We hope this can be very useful in dilute systems.

Any cluster is representative because the mass dispersion is very small. As an example, we compare the ratio N_p/N_o (N_p and N_o are the number of experiments performed in the perimeter and optimized models, respectively) when both models are simulated to achieve nearly the same relative standard deviation $\Delta M/M$. The results are shown in Table II.

For one-to-one realization, we have already compared the optimized algorithm to that of the ordinary invasion percolation. The results were even more impressive (see Fig. 6 of Ref. [10]).

As shown in Ref. [10], when $D \in [\frac{91}{48},2]$ it coincides with the usual fractal dimension D_F; if $0<D<\frac{91}{48}$ the system is frustrated in the sense that it tries but fails to invade less than one site; if $D>2$ the system is also frustrated but now for a

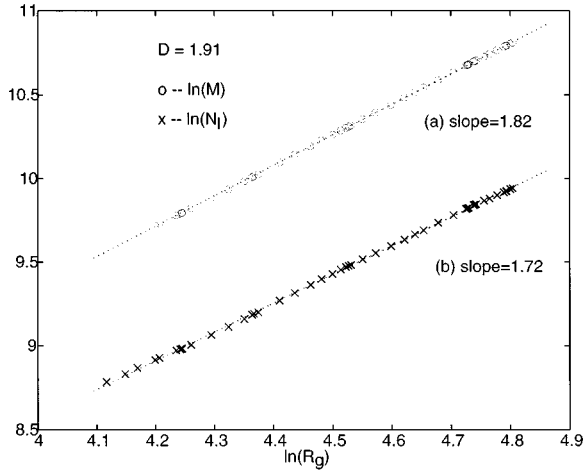

FIG. 2. (a) The symbol *o* stands for the logarithm plot of the backbone mass vs its gyration radius. (b) The logarithm dependence of the backbone loop number N_l with the gyration radius.

different reason: the invasion cannot be faster than allowed by the two-dimensional lattice. In the last two situations $D \neq D_F$.

In this paper we use the optimized algorithm to simulate only *one* cluster. The growth of this unique cluster is stopped each 50 steps. Then we measure the mass and the loop number for both the cluster and its backbone. Their corresponding gyration radius and the minimum path are also determined. At each stage the rectangle in which the cluster is actually inscribed is also obtained (up to lattice size $L=401$). The lattice center and the point P_2 where the cluster touches that rectangle are used to get the minimum path. The elastic backbone is the collection of all these paths. It is a faint structure with almost one-dimensional characteristics. When we pass from one rectangle to the next, usually it happens that P_2 turns, for example, from north to south or east. So in just one step the sites composing the elastic backbone change wildly, precluding its determination (remember that here no averages are made).

We studied the optimized model only in the physical region $D \in [\frac{91}{48},2]$. Below we present our results.

A. The mass

Naturally, $D \equiv D_F$ for the cluster mass. To our surprise the scaling (7) is also perfectly obeyed by the backbone [see Fig. 2(a)]. Remember that Eq. (7) was only imposed on the cluster. In Table III we present the fractal dimensions D_F for some values of D. Remember that we performed only a unique realization. The errors bars correspond to the standard deviation calculated along this experiment. Observe that at $D=1.89$ (the fractal dimension of the ordinary invasion percolation) we get for the backbone $D_F=1.74\pm0.01$, which is greater than the 1.647 ± 0.004 [16] of the ordinary invasion percolation. This means that although the optimized model at $D=1.89$ and the ordinary invasion have the *same* cluster fractal dimension, they are intrinsically different since their backbones are different. Conductivity properties will not be the same.

TABLE III. The scaling exponents of the optimized model. The order they appear in this table corresponds to the cluster and backbone, respectively.

D	D_F	D_l	$D_{\min}$
1.89	1.89	1.74(1)	1.17(8)
	1.74(1)	1.63(1)	
1.91	1.91	1.78(1)	1.05(2)
	1.82(1)	1.72(1)	
1.95	1.95	1.83(1)	1.00(2)
	1.93(1)	1.82(1)	
2.00	2.00(1)	2.00(1)	1.00(1)
	1.99(1)	1.99(1)	

B. The red sites

An astonishing result that we got is that the number of red sites N_r of the optimized model is *very small and random*. It does not obey any power law. For example, when we grow one cluster and count the number of red sites at sizes $L=51,101,151,201,251,301,401$ we find $N_r=1,8,8,1,6,3,7$. To investigate this further, we simulate at $D=1.95$ (just in the middle of the physical region [1.89,2.00]) with lattice sizes $L=51,101,151,201$ and the number of realizations 100,100,60,15, respectively. We got $\langle N_r \rangle = 1.33,1.49,1.43,1.87$. This brings us to the conclusion that for our optimized model the concept of red sites is not important. The number of red sites number is so small that the probability of disconnecting the cluster by removing randomly any site is practically zero. The optimized algorithm destroys the red sites, increasing the cluster connectivity.

C. The loops

The number of loops N_l scales with the gyration radius R_g in the usual way:

$$N_l \sim (R_g)^{D_l}. \tag{8}$$

Looking at Table III we conclude that, as expected, both exponents go to 2 with increasing D.

To see the influence of the ensemble averages on the scaling exponents we have performed 40 realizations of the optimized model on a lattice size $L=251$ and $D=1.91$. We got $D_l=1.73(4)$ for the cluster; $D_F=1.84(1)$ and $D_l=1.70(2)$ for the backbone, and $D_{\min}=1.02(3)$. These results are fairly good when compared to $D_l=1.78(1)$; $D_F=1.82(1)$, $D_l=1.72(1)$, and $D_{\min}=1.05(2)$, respectively, obtained for just one realization on size $L=401$. Unfortunately, we were not able to simulate larger lattices because of the huge CPU demand (a unique $L=401$ realization took 52 h on an Alpha/275 station).

D. The minimum path

The minimum path scales as Eq. (6). Our results are shown in Table III. As in the perimeter model, the exponent $D_{\min}$ approaches 1 as the cluster becomes more compact.

TABLE IV. The abrupt variation of the mass, loops, and red points at the moment of the explosion.

	Cluster		Backbone	
	Before	After	Before	After
Mass	1619	2358	1045	2310
Red points	52	1	52	1
Loops	863	1981	776	1981

E. The burst phenomenon

We already know from Ref. [10] that the system is frustrated when $D \in [0, \frac{91}{48}]$ ($D_F = \frac{91}{48}$) or $D > 2$ ($D_F = 2$). In the last regime the burst phenomenon takes place. This corresponds to an enormous and sudden mass explosion. We simulate at $D = 5.00$ ($L = 201$) just before and after one such explosion (at time step 965, just as in Fig. 11 of the Ref. [10]). The results for the cluster and the backbone are shown in Table IV. It shows a dramatic increase (decrease) of the mass and loops (red sites).

IV. CONCLUSIONS

We use the burning method to identify and analyze the cluster, the backbone, and the elastic backbone structures of the multiple invasion percolation model. We determine the scaling exponents for both the perimeter and the optimized models as well as their dependence with the parameters F and D. For those structures we also study the behavior of the mass, the number of red points, the number of loops, and the minimum path. The optimized model in the physical region $D = D_F \in [\frac{91}{48}, 2]$ exhibited two amazing properties: the perfect scaling of the backbone mass with its gyration radius and the disappearance of red points. This model seems to be well suited to treat dilute systems where the fluctuations of the clusters ensemble hamper the data accuracy and cloud the reality.

ACKNOWLEDGMENTS

We acknowledge CNPq (Conselho Nacional de Desenvolvimento Científico e Tecnológico) and FAPESP (Fundação de Amparo a Pesquisa do Estado de São Paulo) for the financial support.

[1] D. Wilkinson and J. F. Willemsen, J. Phys. A **16**, 3365 (1983).
[2] T. A. Witten and L. M. Sanders, Phys. Rev. B **27**, 5686 (1983).
[3] P. Grassberger and S. S. Manna, J. Phys. (France) **51**, 1077 (1990).
[4] P. Bak, C. Tang, and K. Wiesenfeld, Phys. Rev. Lett. **59**, 381 (1987).
[5] R. N. Onody, A. N. D. Posadas, and S. Crestana, J. Appl. Phys. **78**, 2970 (1995).
[6] D. Wilkinson, Phys. Rev. B **30**, 520 (1984).
[7] A. Birovljev, L. Furuberg, T. Feder, T. Jøssang, K. J. Maløay, and A. Aharony, Phys. Rev. Lett. **67**, 584 (1991).
[8] P. Meakin, J. Feder, V. Frette, and T. Jøssang, Phys. Rev. A **46**, 3357 (1992).
[9] R. N. Onody, Int. J. Mod. Phys. C **6**, 77 (1995).
[10] R. N. Onody and R. A. Zara, Physica A **231**, 375 (1996).
[11] P. G. de Gennes, J. Phys. (France) Lett. **37**, L1 (1976).
[12] H. E. Stanley and A. Coniglio, Phys. Rev. B **29**, 522 (1984).
[13] H. J. Herrmann and H. E. Stanley, J. Phys. A **21**, L829 (1988).
[14] H. J. Herrmann, D. C. Hong, and H. E. Stanley, J. Phys. A **17**, L261 (1984).
[15] D. Laidlaw, G. MacKay, and N. Jan, J. Stat. Phys. **46**, 507 (1987).
[16] P. Grassberger, J. Phys. A **25**, 5475 (1992).
[17] U. P. C. Neves and R. N. Onody, Physica A **218**, 1 (1995).
[18] B. B. Mandelbrot, *The Fractal Geometry of Nature* (Freeman, New York, 1982).
[19] A. Coniglio, Phys. Rev. Lett. **62**, 3054 (1989).